IOP Conf. Series: Journal of Physics: Conf. Series **1037** (2018) 072053 doi:10.1088/1742-6596/1037/7/072053

Comparison of Mean and Dynamic Wake Characteristics between Research-Scale and Full-Scale Wind Turbines

P. Doubrawa, L. A. Martínez-Tossas, E. Quon, P. Moriarty, M. J. Churchfield

National Renewable Energy Laboratory, Golden, CO, USA

E-mail: Paula.Doubrawa@nrel.gov

Abstract. Comprehensive utility-scale wake measurements from commercial wind plants are difficult to obtain. As a result, research in wind farm aerodynamics is often based on smaller-scale measurements and on numerical experiments. It is therefore crucial for the scientific community to understand how results compare across scales. In this work, three actuator-line large-eddy simulations are performed to investigate the sensitivity of mean and dynamic wake characteristics to changes in hub height (for the same turbine model) and in rotor size and properties (for a research-scale and a land-based-scale rotor at the same hub height). Results reveal that ground proximity has a large effect on wake expansion via turbulent transport of axial momentum and on the magnitude of lateral and vertical meandering. The rotor-size experiment suggests that wakes from different-scale turbines expand similarly when not limited by the ground, but that the meandering magnitude is not easily translatable across scales. Finally, the short-rotor wake recovers faster than the tall-rotor wake, but the far wakes of the different-sized rotors at the same absolute height are scalable.

1. Introduction

A wide range of turbulence scales from synoptic weather disturbances to blade-tip vortices directly affect the dynamics of wind turbine wakes. As a result, measurements of these unsteady and inhomogeneous wake flows are often limited in spatio-temporal resolution and extent. Wake characterization studies are challenging even with state-of-the-art instrumentation such as lidars due to the trade-offs between sampled volume size and measurement resolution and to the assumptions made to retrieve flow speed [1]. Therefore, wind turbine wake research should ideally rely on a combination of diverse measurement techniques that can collectively be used to understand wake behavior in the context of freestream atmospheric conditions, as well as the wind turbine aerodynamic properties and operating state.

Such data sets are extremely difficult to obtain. When field campaigns are conducted at operational wind farms, experiments are often constrained to comply with the plant operational strategy and minimize revenue losses. Moreover, the proprietary nature of wind turbine data further complicates the establishment of a comprehensive data base. To circumvent these difficulties, research in wind farm aerodynamics is often based on numerical models and on scaled experiments conducted in wind tunnels or at research-scale (i.e., small utility-scale) wind farms. An example of the latter is the Sandia National Laboratories Scaled Wind Farm Technology

(SWiFT) facility [2], which was specifically designed for research and new technology testing in wind energy. In addition to the SWiFT facility's flexibility to accommodate experiments and its extensive instrumentation, the data collected at the site are freely available, making it an attractive site to a large scientific community.

Although measurements collected at the SWiFT site can be used to inform our knowledge of full-scale wind plant aerodynamics, potential limitations associated with the research-scale nature of the turbines cannot be neglected. These limitations are not yet understood. Particularly, the effect of rotor size and distance from the ground on wake development have not been previously examined. With that in mind, the objective of this study is to investigate the effect of wind turbine hub height and rotor size on mean and dynamic wake characteristics, thereby indicating which observations obtained at the SWiFT site could potentially be carried over to full-scale wind plants with taller towers and larger rotors.

The analysis presented herein is based on numerical experiments. This choice is motivated by the challenges of directly comparing full-scale and research-scale wake measurements obtained at distinct sites in a noncontrollable atmospheric environment and often using different instruments. The results obtained can serve to guide the direction of ongoing research efforts carried out at the SWiFT facility, to provide insight into which quantities of interest best translate to full scale (thus supporting wind turbine wake research, in general) and to inform future measurement campaigns and numerical experiments.

2. Data

The objective of this work is to investigate the effect of wind turbine hub height and rotor size on wake dynamics. To individually isolate these two effects, three wake simulations are conducted. Two of them make use of the same wind turbine model at different tower heights. To accompany this change in tower height, inflow conditions for these two wake simulations (Fig. 1) are generated separately in precursor large-eddy simulations (LES) with periodic lateral boundaries, and targeting the same reference wind speed (7 m s^{-1}) and direction (270°) at their respective hub heights. The turbine considered is the one found at the SWiFT facility: the research-scale V27. The two reference heights are 32 m (`V27.32m`; a typical hub height for this wind turbine) and 80 m (`V27.80m`; a typical hub height for a land-based, full-scale wind turbine). The tall-rotor V27 simulation is also considered in the different-rotor experiment, where it is compared with a wake simulation of a full-scale rotor at the same tower height and subjected to identical inflow conditions. The large rotor is that of a typical land-based-scale wind turbine: the GE 1.5sle (`GE.80m`).

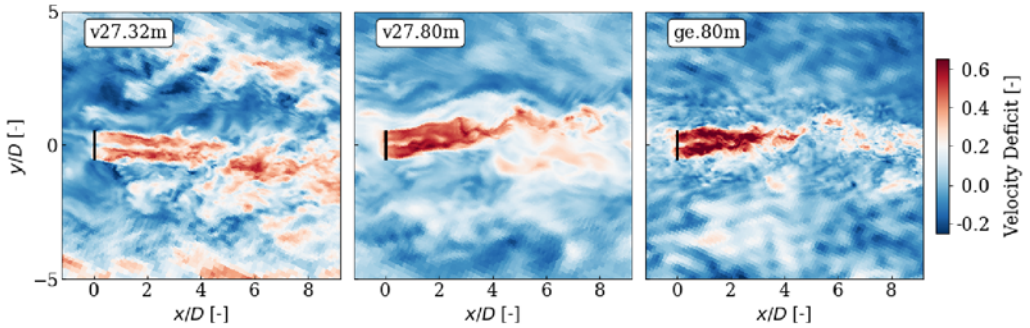

Figure 1: Horizontal snapshot of velocity deficit for simulations `V27.32m`, `V27.80m`, and `GE.80m` at hub height. Note that the mesh grid spacing varies between 0.6 m (in the wake) and 10 m (away from the wake).

These LES were performed with the National Renewable Energy Laboratory (NREL)

Simulator fOr Wind Farm Applications (SOWFA). The two precursor atmospheric boundary-layer (ABL) simulations were forced with a wall-normal heat flux of 0.02 K m s^{-1} into the domain, resulting in unstable atmospheric conditions (thus minimizing the effect of vertical wind shear on wake development). The roughness length was set to 0.15 m. The wall-model friction velocity was on average ~ 0.455 m s^{-1} (for the 32-m precursor) and ~ 0.390 m s^{-1} (for the 80-m precursor). These ABL simulations were then used as initial and boundary conditions for the actuator-line simulations, which are the subject of the analysis.

The total simulation time after spin-up is 20 minutes, and flow fields are saved at 1 Hz frequency. The mesh size is 5 km $\times$ 5 km $\times$ 2 km, and the grid spacing is uniform at 10 m with four refinement zones in the wake where it becomes 0.6 m (seen by the change in spatial resolution in Fig. 1). For these wake simulations (summarized in Table 1), the wind turbine is located in the center of the domain in the spanwise (i.e., lateral) direction, and 1.5 km downstream of the inflow boundary in the streamwise (i.e., axial) direction. The mesh was rotated by 25° off the target wind direction to prevent large-scale flow structures from cycling through the simulation domain in the periodic precursor.

Table 1: Temporally averaged (over the total simulation time of 20 minutes) inflow and turbine operating conditions for the wake simulations: power-law exponent (α_{abl}, computed across rotor top and bottom); hub-height (z_{hub}) wind direction ($\overline{wdir}_{hub}$), speed ($\overline{U}_{hub}$), and turbulence intensity ($\overline{TI}_{hub}$); shear ($\Delta\overline{U}_{rotor}$) and veer ($\Delta\overline{wdir}_{rotor}$) across the rotor; and turbines thrust (C_T) and power (C_P) coefficients and tip-speed ratio (TSR).

	α_{abl} [-]	z_{hub} [m]	$\overline{wdir}_{hub}$ [deg]	$\overline{U}_{hub}$ [m/s]	$\overline{TI}_{hub}$ [-]	$\Delta\overline{U}_{rotor}$ [m/s]	$\Delta\overline{wdir}_{rotor}$ [deg]	C_T [-]	C_P [-]	TSR [-]
`V27.32m`	0.21	32	268	6.7	0.16	1.2	-0.1	0.71	0.49	7.5
`V27.80m`	0.18	80	272	6.8	0.13	0.4	0.0	0.72	0.49	7.5
`GE.80m`	0.18	80	272	6.8	0.13	0.4	0.0	0.83	0.48	8.9

3. Methodology

All data analyzed are on a coordinate system aligned with the planar-averaged, hub-height wind direction (270°), where x, y, z are the streamwise (i.e., axial or rotor-normal), spanwise (i.e., lateral), and vertical (i.e., wall-normal) coordinates given in units of rotor diameters (D) with origin at the hub ($x_{hub}, y_{hub}, z_{hub}$). The analysis is conducted on two-dimensional planes: xy planes at z_{hub} and yz planes for various x at discrete distances upstream and downstream of the rotors. For most of the wake analyses presented herein, data are limited between -2 D and 6 D, at which point the wakes have dissipated substantially and the relative comparisons are no longer meaningful.

Temporal means are notated with an overline (e.g., $\overline{u}$), mean-centered perturbations with a prime (e.g., u'), and spatial averages with angled brackets (e.g., $\langle u \rangle_{xy}$ for an average of u in the xy plane). The quantities analyzed are the LES-filtered flow components (u, v, w), horizontal wind speed (U) and direction ($wdir$), turbulence intensity (TI), turbulent kinetic energy (TKE), and turbulence covariances (e.g., $\overline{u'v'}$). The turbulence quantities are used to diagnose momentum transport and TKE redistribution within the wake and to identify wake recovery pathways.

Wake characteristics are derived from the fundamental flow variables. The velocity deficit (vd) follows the conventional definition of $vd = 1 - u(x, y, z, t)/u_\infty$, where u_∞ is taken as the reference wind speed of 7 m s^{-1}. When analyzing mean fields, the edge of the wake on a yz plane is identified by finding a closed contour that conserves the streamwise momentum deficit using NREL's SAMWICh Toolbox [3]. For individual snapshots where the velocity field is more

complex, a two-dimensional Gaussian-fit approach in SAMWICh is preferred. The wake center is defined as the weighted vd centroid within the wake edge contour. Wake meandering is quantified in terms of wake center motion in these yz planes, both in the horizontal and vertical directions. Wake recovery is analyzed in terms of vd in the planes.

4. Hub-Height Experiment

This section first presents the background flow in which the tall and short V27 turbines operate (Section 4.1), providing a context for the discussion of the main results. Next, the two wakes are characterized and compared in terms of their expansion, recovery, and meandering (Section 4.2). The differences identified from this analysis are then further investigated by considering turbulence characteristics in and outside of the wakes (Section 4.3).

4.1. Upstream Flow and Turbine Operation

Hereinafter, freestream conditions are approximated by the upstream flow at $x = -2$ D. The upstream profiles in Fig. 2 indicate that the inflow is not entirely identical for the two wake simulations. The axial velocities $\overline{u}$ are of approximately the same magnitude at hub height, and they exhibit similar shear across the boundary layer (see power-law exponents in Table 1). As a result, the shorter rotor is subjected to higher shear inflow.

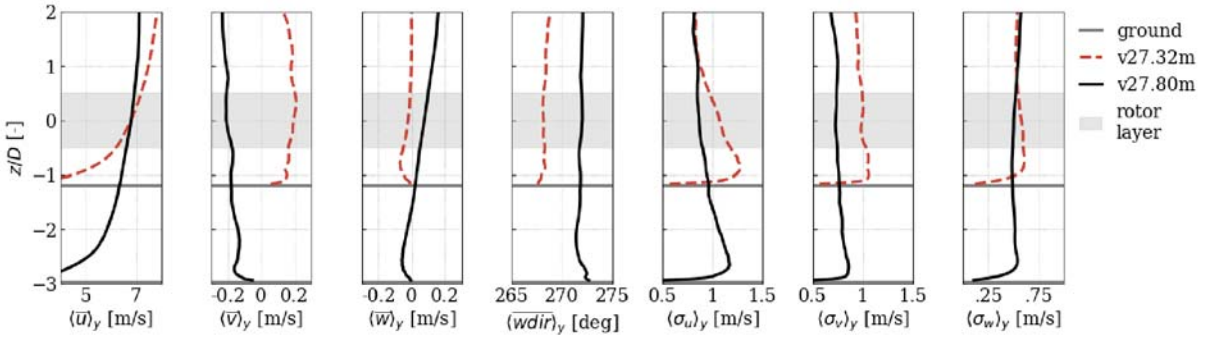

Figure 2: Laterally averaged vertical profiles (for `V27.32m` and `V27.80m`) at $x = -2$ D of temporally averaged streamwise ($\overline{u}$), spanwise ($\overline{v}$), and vertical ($\overline{w}$) flow, and wind direction ($\overline{wdir}$); and of temporal standard deviation of u, v, and w. Horizontal lines mark ground location (a function of z_{hub} and D).

The lateral velocities $\langle\overline{v}\rangle_y$ are positive (negative) for `V27.32m` (`V27.80m`), resulting in a mean yaw misalignment of $\sim |2°|$ and opposite sign in either simulation. These differences suggest that $x = -2$ D may not provide a robust estimate of freestream conditions, or that statistical convergence may not have been reached with the 20-minute simulations. Despite these differences in $\langle\overline{v}\rangle_y$ magnitude, the well-mixed unstable atmosphere results in negligible veer across the rotor in both cases. The total $\overline{v}$ variance is higher for the shorter rotor, which could lead to more meandering for its wake. This hypothesis is investigated in Section 4.3.

In both simulations, the vertical velocities $\langle\overline{w}\rangle_y$ are negative near the ground and close to zero in the lower part of the ABL. This results in $\langle\overline{w}\rangle_y \sim 0$ ($\langle\overline{w}\rangle_y > 0$) in the rotor layer of the short (tall) tower. Once again, this suggests that 20 minutes may not be long enough for assessing flow statistics, which is valuable insight to be addressed in future work. Differences in $\overline{TI}$ are also seen, with the `V27.32m` turbine experiencing higher values due to closer ground proximity. Despite the differences noted herein, the inflow to both turbines is similar enough to ensure matching operating conditions, as shown by the C_T and C_P values in Table 1.

The integral timescale (T) of the inflow turbulence was estimated from the upstream yz flow planes by integrating the auto-correlation functions (for u', v', w') at (y_{hub}, z_{hub}, t) up

to their first zero crossing. As expected, results reveal larger timescales for the taller rotor: $T_{u'} \sim 5.0$ s, $T_{v'} \sim 3.6$ s, and $T_{w'} \sim 3.2$ s (compared to $T_{u'} \sim 4.0$ s, $T_{v'} \sim 3.0$ s, and $T_{w'} \sim 2.4$ s for the shorter rotor), as can also be noticed qualitatively in Fig. 1. These timescales can be translated to integral length scales using the frozen turbulence hypothesis. A relative comparison of the freestream length scales to the rotor diameter can serve as insight to the expected level of wake meandering (driven by scales larger than ~ 2 D) and dissipation (driven by small scales). For reference, $T = 3.9$ s corresponds to a length scale of 1 D for a velocity scale of 7 m s^{-1}.

4.2. Bulk Wake Characteristics

Bulk wake metrics were diagnosed from the flow field for both simulations. Figure 3a shows that the two wakes expand differently as they propagate downstream. The `V27.32m` wake expands more in the lateral direction, acquiring an oblong shape. Its vertical expansion is clearly limited by the ground proximity, as verified by the flat lines marking the bottom edge of the wake at all x. The taller wake of `V27.80m` expands symmetrically in all directions, and its mean shape does not appear to sense the ground.

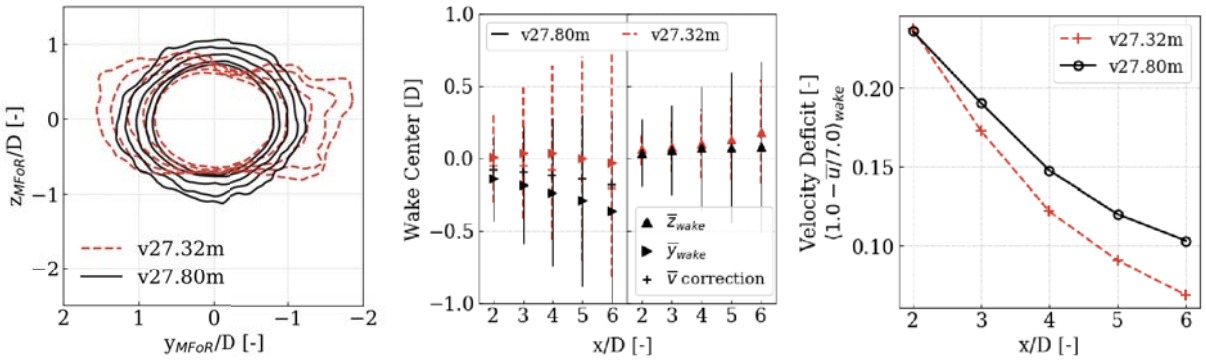

(a) Wake Outline (b) Wake Deflection/Meandering (c) Wake Recovery

Figure 3: Mean wake outline ($x = 2 - 6$ D) in a meandering frame of reference (MFoR) (a); wake center mean (i.e., deflection) and standard deviation (i.e., meandering), with a correction for lateral deflection due to $\overline{v}(z) \neq 0$ at $x = -2$ D (b); and wake-averaged $\langle \overline{vd} \rangle_{wake}$ (c).

The lateral wake deflection appears to be negligible for the short wake, but pronounced for the tall wake (side triangles in Fig. 3b). Because the two simulations were driven with different inflow [i.e., $\overline{v}$ of same value but opposite direction (Fig. 2)], it is difficult to determine with confidence whether these differences in deflection arise from the difference in hub height or in inflow. If $\overline{y}_{wake}$ is corrected for the nonzero, freestream $\overline{v}$, then the differences between `V27.32m` and `V27.80m` become negligible (crosses in Fig. 3b). In the vertical direction, the mean wake deflection is slightly higher for the shorter rotor (the shaft tilt is 4° in both simulations).

Meandering is quantified by one standard deviation of the wake-center time series at each distance downstream. The values shown in Fig. 3b indicate that the wake from the shorter (taller) rotor meanders more laterally (vertically). These results are consistent along the axial direction. Mechanisms for this behavior will be further investigated in Section 4.3 through quantification of turbulence characteristics in the freestream and the wake of both rotors.

Figure 3c shows the downstream evolution of $\overline{vd}$ spatially averaged within the wake outlines of Fig. 3a. From this analysis, it can be seen that the $\overline{vd}$ magnitudes are similar between the two simulations in the near wake, due to similar axial inflow at their respective hub heights. As the wakes propagate downstream, differences become increasingly noticeable, with a faster wake recovery for the shorter rotor. This is likely due to the higher TI and shear experienced

by `V27.32m`, but these mechanisms will be discussed in more detail in Section 4.3.

4.3. Turbulence Upstream and in the Wake
In this section, turbulence properties in and outside of the wakes are investigated to elucidate the physical processes driving the differences in bulk wake characteristics discussed in Section 4.2.

4.3.1. Momentum Fluxes To understand differences in the expansion patterns of both wakes (Fig. 3a) it is useful to investigate differences in the redistribution of axial momentum. In addition to advection and to pressure-gradient and buoyancy forces, the momentum budget is also dictated by turbulent transport. This term can be estimated as the vector

$$\frac{\partial \overline{u'u'}}{\partial x}\hat{i} + \frac{\partial \overline{u'v'}}{\partial y}\hat{j} + \frac{\partial \overline{u'w'}}{\partial z}\hat{k}, \tag{1}$$

with the $\hat{j}$ and $\hat{k}$ terms contributing to the turbulent transport of axial momentum in the lateral and vertical directions, respectively. For the two simulations, the $\overline{u'v'}$ and $\overline{u'w'}$ covariances are the two highest-magnitude terms of the Reynolds stress tensor after $\overline{u'u'}$ and $\overline{v'v'}$.

Figure 4a reveals substantially higher values of $\overline{u'v'}$ for the shorter rotor, indicating that lateral turbulent transport of u' is one of the mechanisms responsible for the pronounced lateral expansion seen in the `V27.32m` wake. The difference in sign for the background values of $\overline{u'v'}$ between the two simulations can be attributed to the differences in $\overline{v}$ previously discussed. The gradient of $\overline{u'v'}$ along y (Fig. 4b) presents quantitative evidence of the larger momentum flux seen at the lateral edges of the wake shear layer for the shorter rotor (negative values indicate momentum increase from turbulent transport). This difference is most pronounced in the near wake. Beyond $x = 3$ D, the mean magnitude of $\partial_y \overline{u'v'}$ is similar for both wakes, and only the lateral offset of the profiles seen in Fig. 4b persists. This offset is likely due to the $\overline{v}$ differences.

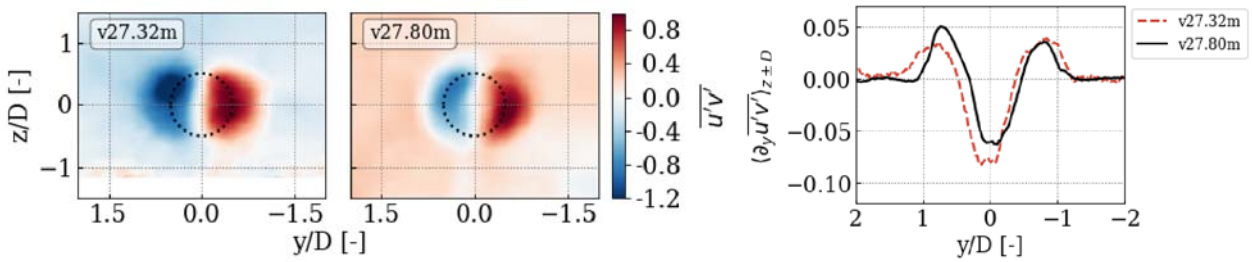

Figure 4: Shear stress $\overline{u'v'}$ (a) and its lateral gradient averaged between $z \pm 1$ D (b) at $x = 2$ D for `V27.32m` and `V27.80m`.

Conversely, Fig. 5a indicates higher values of $\overline{u'w'}$ for the taller rotor, especially at the bottom of the wake. The vertical turbulent transport of u' contributes to the redistribution of axial momentum, and these larger values can partly explain the vertical wake expansion seen in `V27.80m` but not in `V27.32m`. The ground proximity appears to inhibit the enhancement of $\overline{u'w'}$ for the shorter rotor. The vertical gradient of this flux averaged between $y \pm 1$ D is shown in Fig. 5b and reveals stronger gradients in the center of the wake and the bottom edge of the wake shear layer. The magnitude of these differences is noticeable throughout the downstream distances considered (not shown).

4.3.2. Energy Spectra To understand the differences in meandering seen in Fig. 3b, energy spectra are estimated for the fluctuating velocities upstream and in the wake. Each curve in

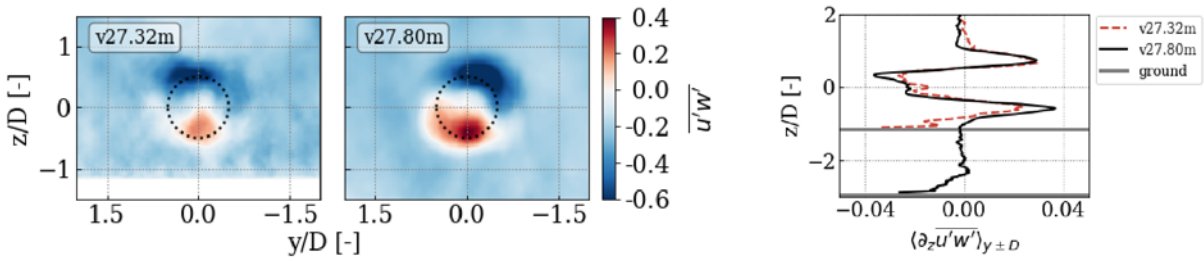

(a) (b)

Figure 5: Shear stress $\overline{u'w'}$ (a) and its vertical gradient averaged between $y \pm 1$ D (b) at $x = 2$ D for `V27.32m` and `V27.80m`.

Fig. 6 was obtained by averaging 121 power spectrum (PS) curves (with a Hanning window of 120 s applied to each), each for a different point in a given yz plane (at a fixed x) on an 11×11 grid centered at the hub and with a total extent of $D/4$ in the y and z directions. This averaging step results in a smooth PS curve for each downstream distance, thus facilitating relative comparisons. The selection of a small area around the origin ensures that the averaged PS values obtained are representative of conditions inside the wake (or of the incoming flow to the rotor, in the case of $x = -2$ D).

The PS of all three components upstream of the rotor is consistently higher (i.e., across all frequencies) for the `V27.32m` simulation, confirming that the shorter rotor experiences more turbulence due to its ground proximity. In the wake, the low-frequency PS values for u' and v' are larger for `V27.32m`, explaining the larger level of lateral meandering seen for the shorter rotor in Fig. 3b. The larger level of vertical meandering seen for `V27.80m` can also be explained by comparing the low-frequency (i.e., at a timescale ≥ 30 s) PS values of w' between the two simulations across downstream distances. Such a comparison reveals that starting at $x = 0$ D, the w' low-frequency energy content in the wake of the taller rotor becomes higher than that of the shorter rotor. This difference becomes more pronounced with downstream distance as the low-frequency energy in w' increases (decreases) for `V27.80m` (`V27.32m`).

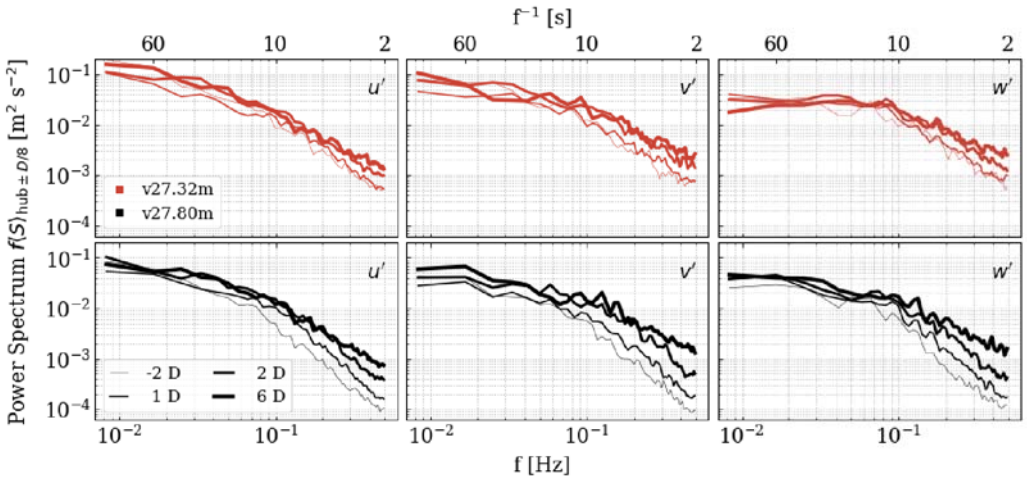

Figure 6: Spatially averaged power spectra for `V27.32m` and `V27.80m` considering an 11×11 grid of points in the yz plane and centered at (y_{hub}, z_{hub}).

A more direct comparison of the downstream evolution of the spectral energy content between

the two simulations can be obtained by integrating the PS values in Fig. 6 across low- and high-frequency bands. The cut-off value between these two bands is taken as $t_{cutoff} = 20$ s. These integrated values are estimates of the variance of large and small turbulent structures in the flow. These values are shown in Fig. 7 and reveal that both simulations show a very similar evolution of $\sigma^2_{u'}$ along x across the spectrum, with the variance of the shorter rotor being consistently larger.

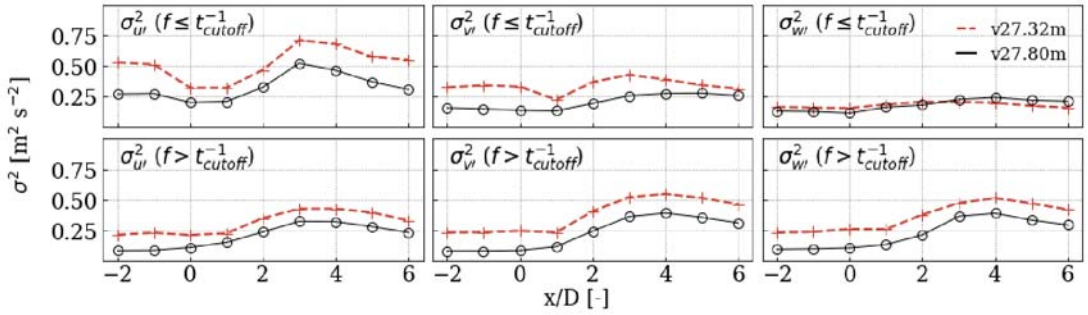

Figure 7: Downstream evolution of velocity perturbations variance as estimated by integrating the PS in Fig. 6 for two frequency bands: below (top) and above (bottom) $t_{cutoff} = 20$ s.

The axial trends in $\sigma^2_{v'}$ are also similar for both simulations, with a sharp increase in the variance of low and high frequencies beyond $x = 1$ D, a peak between 3 and 4 D, and a recovery signal beyond that. As mentioned, the consistently higher values of v' variance in the shorter rotor simulation are the likely cause for its larger lateral meandering. Likewise, the larger values of low-frequency $\sigma^2_{w'}$ for the tall rotor beyond $x = 3$ D could partly explain the larger vertical meandering seen for `V27.80m`. Despite these differences for the low frequencies, Fig. 7 reveals that the addition of TKE at small scales is comparable for both simulations (i.e., the high-frequency variance curves track together for the three velocity components).

5. Different Rotor Experiment

This experiment considers simulations `V27.80m` and `GE.80m`, both of which are driven with identical inflow conditions, which are given in Fig. 2. For `GE.80m`, only the normalization of the coordinates would change due to a different D value. At the hub-height wind speed considered, the two rotors operate at slightly different thrust (Table 1). This result reflects the challenge in exactly matching operating conditions in actuator-line LES of two different turbine models. These differences in thrust further complicate the comparison of wakes generated by rotors with different aerodynamic properties, and the analysis presented herein therefore focuses on quantities that are affected more by inflow and rotor size (i.e., meandering and expansion) than by thrust (i.e., vd and wake recovery).

Figure 8a shows the bulk wake characteristics for both simulations, revealing an azimuthally symmetrical expansion pattern for both wakes, but a more rapid expansion rate for the smaller rotor. Figure 8b indicates that the smaller rotor meanders more in both directions (y and z), but that its mean centerline is deflected slightly less than the the centerline of the large rotor. Note that the meandering magnitude is larger for the larger rotor in Fig. 8b; but in dimensional form it is actually smaller because the presented values are normalized by D. Fig. 8c gives the wake-averaged $\overline{vd}$ normalized by its value at $x = 2$ D. This normalization is done to reduce the effect of different thrust on the results, and reveals that both wakes recover at a similar rate beyond $x = 2$ D.

Figure 9 presents the downstream evolution of the variance of each velocity perturbation component and is analogous to Fig. 7. The main difference here is that the cut-off frequency for integrating the hub PS is different for each rotor based on its diameter ($t_{cutoff} = 2$ D/7.0 m s^{-1}).

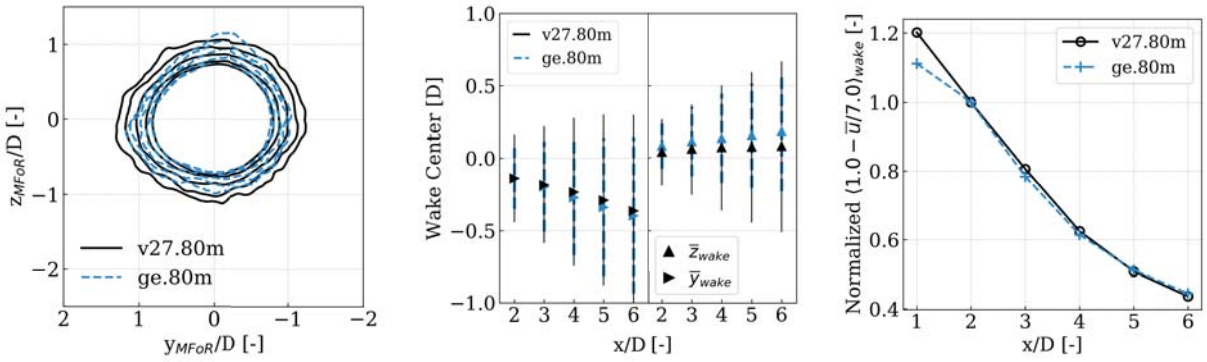

(a) Outline (b) Deflection and Meandering (c) Recovery

Figure 8: Mean wake outline in a meandering frame of reference (a), mean wake center and meandering (b), and wake-averaged $\overline{vd}$ (c) for $x = 2 - 6$ D for `V27.80m` and `GE.80m`.

We see that at low frequencies, the values are similar for both simulations for $x \leq 0$ D. After going through the rotor, the large-scale u' variance sharply increases and decreases for the large rotor but only gradually increases for the small rotor. More pronounced differences are seen for the lateral and vertical flow components. Namely, the large-scale variances of the small rotor remain fairly constant whereas those of the large rotor see a sharp spike at $x = 3$ D, followed by a decrease to the original, upstream value by $x = 6$ D (the same trend is seen for various choices of t_{cutoff}).

Upon analysis of these results, one might expect more centerline meandering for the larger rotor. The fact that this is not seen (Fig. 8b) suggests that the ratio between the integral length scale in the inflow to the rotor diameter is an important parameter that should be considered in meandering analyses. Here, the inflow is identical and the rotor sizes are different, so this ratio is smaller for `GE.80m`, causing it to meander less than `V27.80m`. At high frequencies, both wakes see an increase in the variance of the three velocity components of approximately the same magnitude, followed by a return to their respective upstream values by $x = 6$ D. The main difference is a consistent delay in the increase of these variances for the smaller rotor.

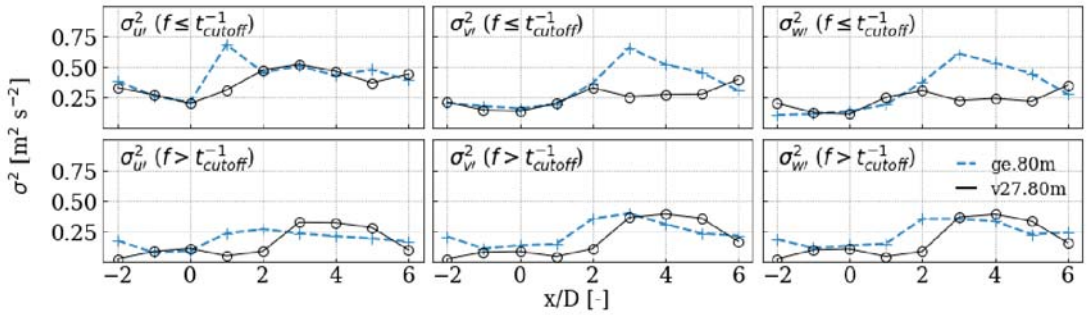

Figure 9: Downstream evolution of velocity perturbations variance as estimated by integrating the PS of `V27.80m` (Fig. 6) and `GE.80m` (not shown) for two frequency bands: below (top) and above (bottom) $t_{cutoff} = (2 \text{ D}/7.0 \text{ m s}^{-1}) \sim 22$ s for `GE.80m` and ~ 8 s for `V27.80m`.

6. Conclusions

The sensitivity of wake development and evolution to wind turbine hub height and rotor size were investigated individually by performing numerical experiments in which research-scale and full-

scale wind turbines were simulated with rotating actuator lines within LES. The main objective of the analysis was to indicate which measurements collected in wakes of research-scale wind turbines can potentially be carried over to full-scale wind plants.

The hub-height experiment revealed that ground proximity has a large effect on lateral and vertical wake expansion via turbulent transport of axial momentum, with the shorter rotor expanding primarily in the lateral direction and the taller rotor exhibiting an azimuthally symmetrical expansion pattern. Due to its ground proximity, the short rotor is in a more turbulent, higher shear environment. Turbulence analyses of the freestream and the wake reveal larger variance of the low-frequency lateral velocity perturbations, resulting in more cross-stream meandering for the lower wake. Conversely, the tall-rotor wake meanders more vertically, which is likely related to the larger low-frequency variance of the vertical velocity perturbations in its wake. A comparison of the velocity deficit evolution between both wakes shows similar intensity in the near wake, but a faster recovery for the shorter-tower wake beyond $x = 2$ D.

The rotor-size experiment indicated that once the ground-proximity effect is removed, both rotors expand symmetrically in the yz planes and the expansion is faster for the small rotor. The large rotor was found to meander less, likely because the ratio of rotor diameter to the inflow integral length scale decreases with increasing rotor size under fixed inflow conditions. The absolute magnitudes of velocity deficit were not compared in this experiment due to the slightly different thrust coefficients of both turbines. Instead, the velocity deficit values were normalized and their evolution revealed an identical recovery rate for both wakes beyond $x = 1$ D.

The results obtained with this work are useful to the scientific community when using relatively small-scale experiments to understand aspects of mean and dynamic behavior downstream of full-scale wind turbines. Insight from this work can be used to guide future numerical and measurement experiments. Ongoing work seeks to extend the analysis presented herein to consider other atmospheric stratification scenarios and a longer simulation time. The analysis will also be refined by computing turbulence spectra and fluxes in a meandering frame of reference to ensure that the meandering signal is not present in wake-recovery analyses. Finally, wake measurements collected at NREL for the full-scale rotor (and at SWiFT for the research-scale rotor) will be used to validate the results obtained in the numerical experiments.

References

[1] Lundquist J K, Churchfield M J, Lee S and Clifton A 2015 *Atmos. Meas. Tech.* **8** 907–920 ISSN 1867-8548 URL `http://www.atmos-meas-tech.net/8/907/2015/`

[2] Kelley C L and Ennis B L 2016 SWiFT site atmospheric characterization Tech. Rep. SAND2016-0216 Sandia National Laboratories (SNL-NM), Albuquerque, NM (United States) dOI: 10.2172/1237403 URL `http://prod.sandia.gov/techlib/access-control.cgi/2016/160216.pdf`

[3] Quon E 2017 Simulated And Measured Wake Identification and CHaracterization URL `https://github.com/ewquon/waketracking/`

Acknowledgments

The authors thank Jason Jonkman from NREL and Thomas Herges from Sandia National Laboratories for contributing in discussions and reviewing the manuscript. The Alliance for Sustainable Energy, LLC (Alliance) is the manager and operator of the National Renewable Energy Laboratory (NREL). NREL is a national laboratory of the U.S. Department of Energy, Office of Energy Efficiency and Renewable Energy. This work was authored by the Alliance and supported by the U. S. Department of Energy under Contract No. DE-AC36-08GO28308. Funding was provided by the U.S. Department of Energy Wind Energy Technologies Office. The views expressed in the article do not necessarily represent the views of the U.S. Department of Energy or the U.S. government. The U.S. government retains, and the publisher, by accepting the article for publication, acknowledges that the U.S. government retains a nonexclusive, paid-up, irrevocable, worldwide license to publish or reproduce the published form of this work, or allow others to do so, for U.S. government purposes.